Design and test of a model Wilkinson combiner for application to a future plasma haloscope

Aaron Schwan

Abstract

In this thesis, I will motivate the use of a broadband Wilkinson junction in a plasma haloscope, a proposed apparatus sensitive to axionic dark matter [9, 11]. I will then review the basics of Wilkinson junctions solving the ideal scattering values and scattering parameters for a single-stage Wilkinson junction as an example. With these in hand, I will then show two common ways of extending the usable bandwidth of the device. The last method discussed for expanding the bandwidth of the Wilkinson junction is based on the same topology used by and diving more fully into a possible scheme to modify a current design employed by Elsbury et al. in a similar frequency and noise required application [4]. Finally, I describe the analysis, construction, and testing of a lower-frequency Wilkinson junction device as a proof of concept and show that the effective bandwidth has increased while not increasing the space required on the chip.

Committee Members
Advisor: Prof. Konrad Lehnert, Physics
Honors Member: Prof. Jun Ye, Physics
Out of Department: Prof. Adam Norris, Applied Mathematics
Defense Date: April 4th, 2023

Contents

List of Figures

1 Motivation for Axions

There is a well-known problem: there is more mass in the universe than can be explained simply by the observed matter. This extra mass, or dark matter, is a significant gap in our understanding of the universe. Another problem in particle physics is known as the strong-CP problem. In this problem, it is noted that our current understanding of physics with the standard model requires an implausible fine-tuning of parameters to explain why the combined charge parity CP symmetry is preserved for the strong nuclear force but is broken in the weak sector. This is where the axion comes in. Initially motivated by solving the strong-CP problem, Peccei and Quinn proposed an extension to the standard model incorporating an anomalous spontaneously broken $U(1)$ symmetry [12]. Weinberg and Wilczek later showed that this broken $U(1)$ symmetry would create a new light spin-0 particle, now called the axion [18, 17] This exciting insight was advanced again by Preskill, Wise, and Wilczek, showing that if the axions are produced early in the lifespan of the universe, they could also be abundant enough and minimally interacting enough to be consistent with properties of cold dark matter [1, 15].

The first problem with proving (or falsifying) the existence of axions is that current theories do not tightly constrain the particle's rest mass. Instead, astrophysical observations and additional hypotheses bound it to a range of possible masses. The mass appears to be on the order of $1\,\mu\mathrm{eV} \lesssim m_a c^2 \lesssim 1000\,\mu\mathrm{eV}$ [7, 6]. Second, they are extremely weakly interacting light particles, so much so that the axion is commonly referred to as the "invisible axion." Nevertheless, the axion would couple to electromagnetism ("photons."), where the coupling takes the form $a\vec{E}\cdot\vec{B}$, with a, $\vec{E}$, $\vec{B}$ the axion, electric, and magnetic field strengths, respectively.

These two aspects of axion physics led to a unique detector concept called a *Haloscope*, which consists of a tunable microwave cavity cooled to ultralow temperatures and embedded in a large, uniform, and static magnetic field. The static magnetic field causes a resonant conversion of the axion field into a spatially uniform (within the cavity) electric field oscillating at $\omega_a = m_a c^2/\hbar$, the axion's Compton frequency. [16]. If the cavity is near-resonant with ω_a, the axions are converted into a narrowband microwave signal that can just barely be detected with quantum-limited amplification methods above a background of quantum fluctuations and residual thermal noise.

The signal power is proportional to the overlap of the electric field of the cavity mode $\vec{E}_{\mathrm{cav}}(\vec{r})$ with the spatially uniform electric field generated by the magnetic field and the axion field $\vec{E_a}$ as $P \propto \int_V \mathrm{d}\vec{r}\,\vec{E}_{\mathrm{cav}}(\vec{r})\cdot\vec{E_a}$, with V the cavity volume. Note that the integral would be zero for many of the resonant modes of a right circular cylinder. Only the TM_{010} mode has substantial coupling.

Furthermore, this expression shows the unfavorable scaling of the axion signal power with increasing frequency. Doubling the frequency reduces the cavity mode volume and the signal power by a factor of eight as higher frequency ranges are searched. From new research by Buschmann, the most plausible frequency for the axion community to scan is around 15 GHz [2]. This high frequency makes it difficult for traditional cavity haloscopes (which have had their greatest success around 1 GHz) to reach the sensitivity needed to detect an axion signal [3].

1.1 Plasma Haloscope

The plasma haloscope is a concept that overcomes this unfavorable scaling by breaking the relationship between resonance frequency and cavity volume. A plasma haloscope works off the property that photons acquire an effective mass inside a plasma. This property does not require a natural plasma but can instead be based upon an effective plasma-like dispersion relation created by a wire metamaterial (or photonic bandgap material) [13]. Looking at Fig. 1, we can see a simple square lattice with spacing a. It is easy to imagine that the lattice will resonate at a specific frequency, and when we imagine an infinite square lattice, it can be solved analytically. Eqn. 1 from Pendry et al. work with *Low-frequency plasmons in thin-wire structures* shows that the frequency scales up approximately with the inverse of the lattice spacing [13]. In Eqn. 1, it is imagined that the wires are infinite length with a radius r and spacing a. It is assumed that c_0 is the velocity of light in free space, n_{eff} is the effective electron density within the lattice, and m_{eff} is the new effective mass of the electrons from being in the plasma.

$$\omega_p^2 = \frac{n_{\text{eff}} e^2}{\epsilon_0 m_{\text{eff}}} = \frac{2\pi c_0^2}{a^2 \ln(a/r)} \tag{1}$$

Equation 1: Plasma frequency, ω_p, of a square lattice of conductive material with a spacing constant a [13].

With a plasma frequency, Maxwell's equations for axions can be solved by assuming an electric field in a linear media with a dielectric constant ϵ. Lawson et al. show that the expected field becomes Eqn. 2.

$$\vec{E} = -\frac{g_{\alpha\gamma}\vec{B}_e a}{\epsilon} = -g_{\alpha\gamma}\vec{B}_e a \left(1 - \frac{\omega_p^2}{\omega_\alpha^2 - i\omega_\alpha \Gamma}\right)^{-1} \tag{2}$$

Equation 2: Expected electric field due to a coupled axion in an infinite thin rodded metamaterial. Found by approximating the material as a linear dielectric and using the Drude model to find the cyclotron frequency [9].

In Eqn. 2, Lawson has defined ω_α as the weakly oscillating axion field, $g_{\alpha\gamma}$ as the coupling constant of the axion, $\vec{B}_e$ as the applied magnetic field and, Γ as the small damping rate that sets the lifetime of the plasmon.

This relation shows us that as the plasma haloscope approaches the same frequency of the axion, we will have a vanishingly small denominator causing a spike in the expected electric field along with the power out. We also see that the electric field proportionally increases as the magnetic field increases. This motivates the tunable plasma haloscope within a strong magnetic field.

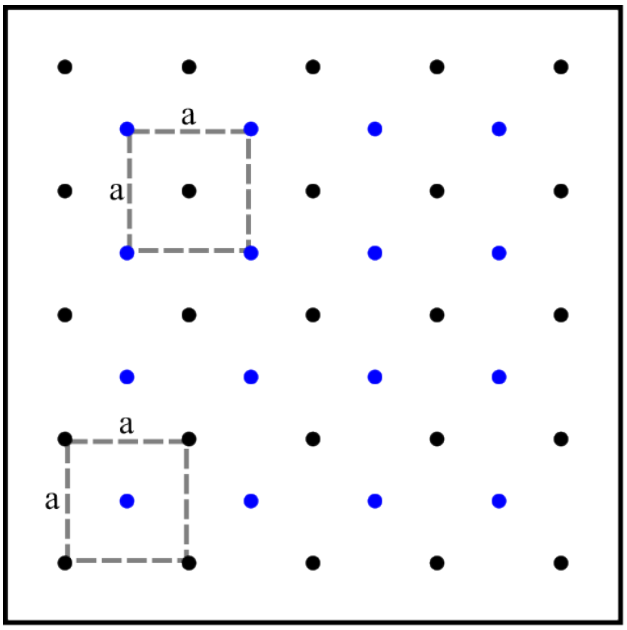

Figure 1: A simple diagram of a plasma haloscope. In this image, a boundary of conducting walls is shown by the solid-lined, rectangular box surrounding the lattice of ports and wires. The wires creating the metamaterial for the plasma haloscope are depicted as black circles in a lattice with a spacing constant a. The antennae are depicted in a blue sub-lattice which could consist of simple monopole antennae.

From Fig. 1, we see a finite lattice formed by the black dots equally spaced and representing a potential version of a plasma haloscope. We are then considering the limit of the plasma haloscope when we have an approximately infinite metamaterial. In this limit, we will need multiple antennae to avoid breaking discrete translational symmetry, which has the potential to hybridize the mode with strong axion coupling with the many uncoupled modes yielding a vanishingly effective coupling for any particular mode. The multiple antennae may also be necessary to improve the coupling of the haloscope to the amplification of the output power [11]. We then propose a binary tree model that reduces the number of ports by the power of the number of input ports of each combiner. This is demonstrated in Fig. 2.

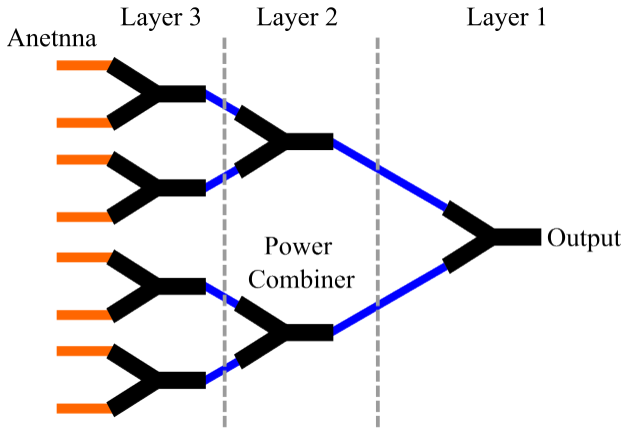

Figure 2: Simple binary tree showing the reduction of eight input ports to a single output port for amplification. Antennae that couple with the cavity are shown in orange, power combiners are shown in black, blue represents transmission lines connecting power combiners, and layers are separated by gray dashed lines.

We are interested in the amount of Wilkinson junctions that are needed for the final plasma haloscope, we can simply look at the rows of the binary tree and divide the number of ports per row by the number of ports of the Wilkinson junction.

$$S(n) = \sum_{i=1}^{\log_j(n)} \frac{j^i}{j} = \frac{n-1}{j-1} \tag{3}$$

Equation 3: Geometric sum showing the relation between the number of ports a power combiner has, j, and the number of ports we are trying to match for input, n.

In Eqn. 3, we have set *j* to be the number of input ports and *n* to be the number of antennae in the plasma haloscope. In this equation, *n* is a power of *j*. We constrain it so that every combiner contains the same number of ports. Setting $j = 2$, we can look at three port combiners, two input ports, and one output summing the values in the binary tree. This relatively common topology is related to a common three-port Wilkinson junction. A three-port combiner, of course, is not a design constraint on the actual haloscope but just a method to obtain the approximate order of magnitude for the number of combiners that will be needed within the binary tree. The number of levels of the binary tree is vital because the more components the wave must travel through, the more potential losses there are in the already weak signal. Using an arbitrary but reasonable lattice size of a 17×17 square plasma haloscope will have 289 individual wires forming the haloscope and a 16×16 lattice of ports connecting to the plasma haloscope, meaning we will have to have a binary tree of 255 Wilkinson junctions. This scale is a reasonable approximation for the scale of a lattice seeing as a copper prototype with a 16×16 wire array has been built at Stockholm

University[8], and a 10×10 wire array has been built by Karl Van Bibbers Group at Berkley [11]. Due to this array scaling in size rapidly, we are interested in on-chip solutions for Wilkinson junctions focusing primarily on bandwidth and size on the chip.

2 Wilkinson Junction Introduction

Wilkinson Junctions are one of the simplest power combiner and splitter topologies and have been an essential tool in the pocket of RF(Radio Frequency) engineering since the 1960s when Ernehest J Wilkinson bridged the ports on a T-splitter using a resistor. This simple modification to a 3-port T-splitter gives us the ability to have isolation between the symmetric ports [19].

Traditionally Wilkinson junctions have been used to split low-power signals either equally among amplifiers or unequally for measurements. They are very effective in this use. However, for our case, we are interested in combining in-phase signals to reduce the necessity for multiple cryogenic transmission lines to connect to a superconducting amplification setup. This would reduce the complexity of the overall design of the amplification setup for a plasma haloscope while maintaining the signal of the haloscope. Because of this, the goal of this section is to act as an introduction to equal split Wilkinson junctions and suggest potential parameters for a Wilkinson junction binary tree with a plasma haloscope.

In this section, we will start by looking through the derivation of *ideal* components for the original single-stage Wilkinson junction and the properties that make up an equal-split Wilkinson junction [19]. With these solutions in hand, we will then show a method using ABCD parameters extended to allow parallel components and allow us to solve for a three-port topology [10]. With the scattering parameters in hand, we can then discuss the bandwidth of the device as well as the common multistage solution to extend the usable bandwidth for the device. We then will show that placing a quarter-wave transformer on port-1 will result in a larger bandwidth. However, we then can detune the parameters allowing us to extend the bandwidth once more. With the detuned parameters, we can test the theory experimentally and show that this is a valid method for extending the usable bandwidth while maintaining an equal amount of space on the chip.

2.1 Ideal Single Stage Wilkinson Junction

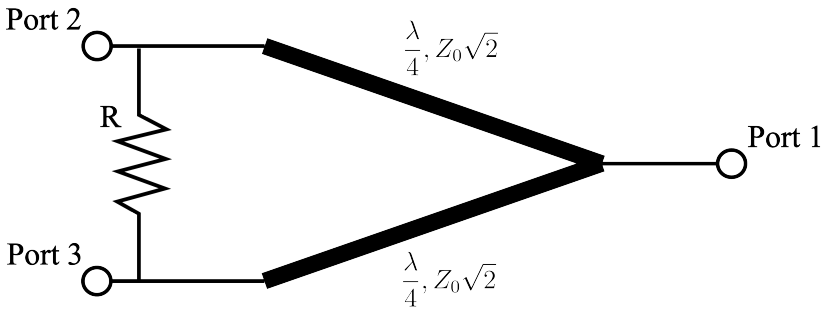

Figure 3: Microstrip diagram of a single stage Wilkinson junction. This three-port combiner consists of input ports 2 and 3 and output at port-1.

The simplest form of a Wilkinson junction is performed using two quarter-wave transformers and a resistor. This is shown in Fig. 3. In this figure, we can see that there are only three components: two quarter wave transformers and a resistor. By defining the ideal natural frequency of the device and the impedance of the ports, we can solve for a power combiner and splitter that work as intended only at one frequency. The Wilkinson junction is desirable over a resistive splitter, especially in applications where we want low loss because of the higher isolation that comes from the resistor bridging the two-quarter wave resonators.

In Fig. 3, we can observe there are two paths from port-2 to port-3. In the simple case assuming that the resistor adds no phase delay while a wave passes through it from port-2 to port-3, we then also have the situation where a wave passes from port-2 to port-3 through two quarter-wave transformers. At this one wavelength, the two methods of traveling from port-2 to port-3 result in the destructive combination of two equal waves 180 degrees out of phase from each other. This leads to the isolation working at one frequency, causing the zero for S_{23} and S_{32}.

It is beneficial for our understanding of the chosen component values for a Wilkinson junction to look at the desired characteristics of the device. Because this is a three-port microwave object, we cannot maintain a lossless, reciprocal, and matched device. Instead, we choose to make a device that is reciprocal and matched, letting us designate it as a power splitter and combiner. First, a matched input of the ports and the Wilkinson junction determines that we have zero reflection at the ports on the natural frequency. Second, Wilkinson junctions have reciprocity. By looking at Fig. 3 a physical symmetry argument we can be made where in $S_{12} = S_{13}$, $S_{32} = S_{23}$, and $S_{22} = S_{33}$. By exploiting the reciprocal nature, we can also say that $S_{12} = S_{21}$ and $S_{13} = S_{31}$. These two constraints have already done a great service in solving the scattering matrix of an

ideal Wilkinson junction.

$$\begin{pmatrix} S_{11} & S_{12} & S_{13} \\ S_{21} & S_{22} & S_{23} \\ S_{31} & S_{32} & S_{33} \end{pmatrix} = \begin{pmatrix} 0 & S_{12} & S_{12} \\ S_{12} & 0 & S_{23} \\ S_{12} & S_{23} & 0 \end{pmatrix} = \frac{-\imath}{\sqrt{2}} \begin{pmatrix} 0 & 1 & 1 \\ 1 & 0 & 0 \\ 1 & 0 & 0 \end{pmatrix} \tag{4}$$

Equation 4: Standard scattering parameter matrix shown on the left is then reduced using reciprocity. On the right is the ideal scattering parameter matrix for a power combiner.

From Eqn. 4, we can define a few more simple positions for an ideal Wilkinson junction, such as seen in the last matrix of the above equation. We desire complete isolation at the natural frequency of the Wilkinson junction. Therefore, in the ideal case, we will have $S_{23} = 0$ because this means that no power is transferred to port-3 from port-2 and vice versa. We also desire an equal split Wilkinson junction, which will lead to half the power transmitted through each input port. This means we will have the scattering parameters $S_{12} = -3$ dB, corresponding to half-power transmission.

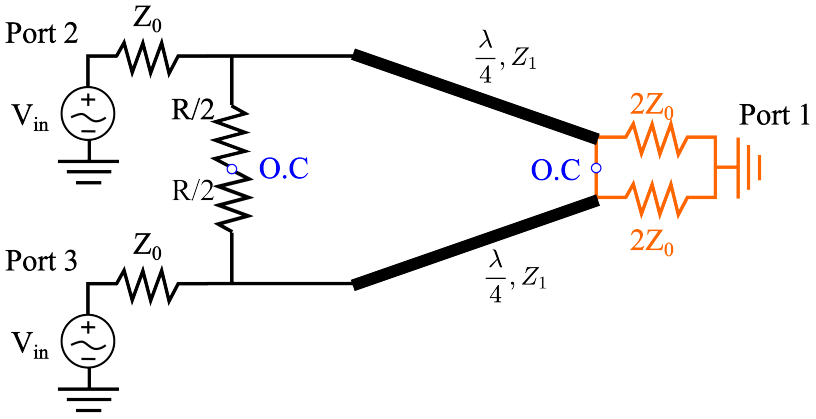

(a)

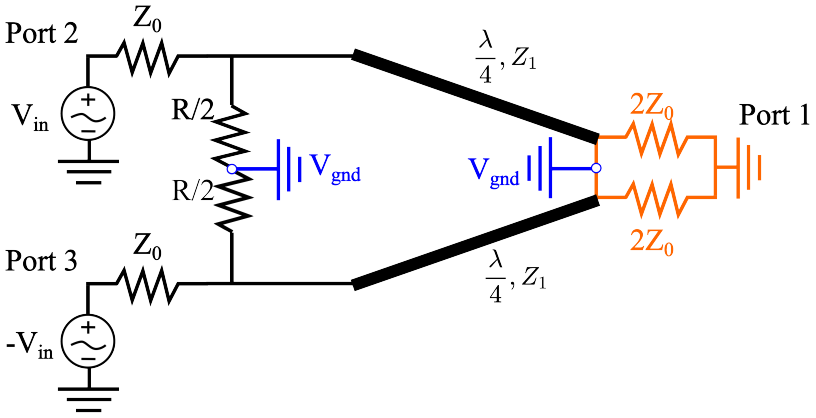

(b)

Figure 4: Even and odd mode analysis modified diagrams from Pozar Microwave Engineering [14]. Even mode analysis is shown in (a) odd mode analysis is shown in (b). The expected virtual ground and a virtual open circuit are shown in blue. To solve for the scattering parameters, we have broken port-1 into two resistors that, in parallel, have the same characteristic impedance as shown in orange.

To solve for the parameters of the Wilkinson junction, we have two different cases where the voltage input to both ports is the same, even mode analysis, and when the voltage input to both ports is 180 degrees out of phase, odd mode analysis. These two cases are shown in Fig. 4a and Fig. 4b. For even mode analysis, there is no potential difference across the resistor, and therefore, it acts as an open circuit as depicted in Fig. 4a. The same argument can be made when talking about how the even modes act at port-1 until the power can go to the ground. These open circuit points

are depicted by blue circles in the circuit diagram. We can then solve the voltage at each of the points of the even mode analysis using the equation for transmission line impedance. From Pozar, we can calculate the apparent resistance, shown in Eqn. 5. We start with $2Z_0$ as the load resistance and the resistance of the transformer as defined in the circuit. We can see that it reduces to the characteristic impedance of the ports showing a matched impedance value. Within Eqn. 5, we can see that we can reach the desired characteristic impedance for the quarter wave transformer by setting the resistance of the transformer to $\sqrt{2}Z_0$.

$$Z_{in} = \frac{Z_1^2}{2Z_0} = \frac{(\sqrt{2}Z_0)^2}{2Z_0} = Z_0 \tag{5}$$

We can then simply find the voltage of the even mode at port-2 by simply using a voltage divider circuit with equal impedance. We will have half the voltage at port $V_{2e} = V_{in}/2$. This is also the same voltage as at port-3 due to symmetry. We will follow the convention denoting the voltage at a port for an even mode with V_{je} and the voltage at a port for an odd mode port with V_{jo} where j is the port being probed in both modes. Because of the phase delay across the transmission line, we will acquire an imaginary term for the voltage at port-1 which is reduced by the apparent resistance to $V_{1e} = -\imath/\sqrt{2}$.

For odd mode analysis, we have two out-of-phase waves resulting in virtual grounds shown in Fig. 4b depicted in blue. As we can see on the right-hand side, this virtual ground appears at port-1, which means we can easily declare $V_{1o} = 0$. Solving for V_{2o}, we can simplify the above circuit as a voltage divider between the two resistors for the port and isolation $V_{2o} = (V_{in}Z_0)/(R/2+Z_0)$ by setting the resistance to twice the characteristic impedance this reduces to half the input voltage. Finally, we can solve for overall voltages by adding the even and odd mode voltages. From even and odd mode analysis, we solve independently for the ideal values.

We can rather simply translate the microstrip definition of a Wilkinson junction to a lumped element model by representing the quarter-wave transformers as lossless π-networks consisting of two capacitors going to ground bridged by an inductor. Using Pozar[14] we can convert the desired frequency response using Eqn. 6 to find appropriate values for the capacitors and inductor in the π-network.

$$\begin{aligned} C &= \frac{1}{Z\omega} \\ L = Z^2C &= \frac{Z}{\omega} \end{aligned} \tag{6}$$

Equation 6: Conversion of microstrip transmission line to a π-network [14].

This π-network simplification can be quickly used to simplify the circuit diagram as Fig. 5. This is important to our design because, at lower frequencies, it becomes practically infeasible. For example, if we desire to combine in the 10 MHz range, we would look for a quarter-wave transformer

approximately 7.5 meters long. This approximation is simply made by dividing the wavelength by four. However, it does illustrate at low frequencies; we need these devices to be significantly smaller. Thankfully we will see that with a lumped element model, we will have a rather small final circuit. For higher frequencies, it is common to transition to microstrip architecture in the GHz range due to the simplicity of the layout and size reduction, with anything over 10 GHz requiring on the order of millimeters of length for the device, which for many applications, is acceptable.

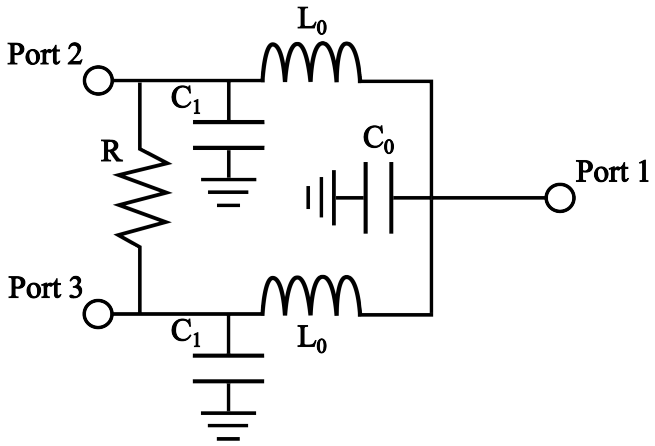

Figure 5: Single-stage lumped element Wilkinson junction circuit diagram.

In the above figure, there is only one other simplification that has been made, which is to differentiate the capacitors into two different values where C_0 is simply $2C_1$.

To solve for the scattering parameters over a broader range of frequencies rather than at a single idealized frequency where there is no reflection, we will use ABCD matrices. Transmission terms can then be solved using an extension of the ABCD matrix for parallel circuits. Because ABCD matrices are only valid for two port circuit topologies, they are first extended to solve for the parallel structure as solved by Levine.

$$ABCD = \begin{pmatrix} \frac{A_1B_2+B_1A_2}{B_1B_2} & \frac{B_1B_2}{B_1+B_2} \\ C & \frac{D_1B_2+B_1D_2}{B_1+B_2} \end{pmatrix} \tag{7}$$

Equation 7: Equation showing the simplification of two parallel components combining to one ABCD Matrix [10]

$$C = \frac{1}{B_1+B_2}(D_1A_2 + D_2A_1 + B_1C_1 + B_2C_2 + B_1C_2 + B_2C_1 - A_1D_1 - A_2D_2) \tag{8}$$

Equation 8: Paired equation for Eqn. 7 [10]

Using Eqn. 7 and Eqn. 8, we can find the solution to the power traveling from each of the ports reducing the network appropriately with a resistor.

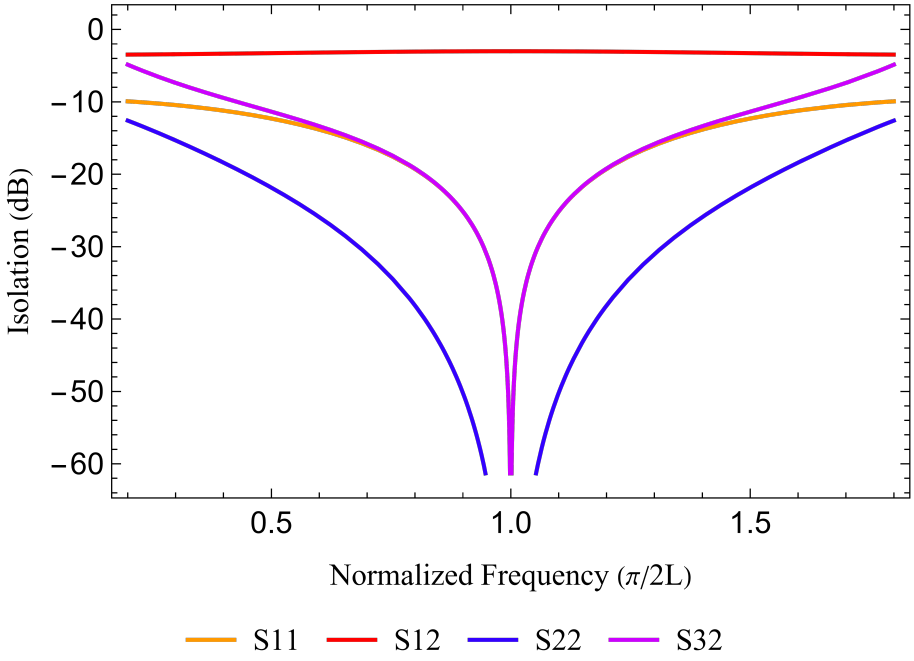

Figure 6: Single-stage Wilkinson junction analytical normalized solution of relevant scattering parameters. A clear natural frequency is observed at 1.0 where five of the relevant scattering parameters become zero and S_{12}, S_{13}, S_{21}, S_{31} are reduced to half the power, -3 dB.

We can use the method outlined by Levine to find the solution to the Wilkinson junction scattering parameters as depicted in Fig. 6. From this graph, we can see that there is a limited bandwidth over which a combiner will be effective. Thanks to the steep drop-off values, the total usable bandwidth of the Wilkinson junction is limited[10].

3 Extending Bandwidth

Depending on our desired applications, several different methods for expanding the bandwidth exist. The three most common methods for expanding the bandwidth for a Wilkinson junction are creating a multistage combiner, changing the isolation resistance, and adding a quarter-wave transformer. The most effective for large bandwidths is a multistage Wilkinson junction where the more stages added to the combiner, traditionally the larger the Wilkinson junction's bandwidth. The next common method is to adjust the apparent resistance of the Wilkinson junction isolation resistor. This is done using different filtering circuits, such as replacing the lone resistor with an RLC circuit. This works well for designing to remove specific frequencies [5]. The issue with this

design is that it has not only added complexity but, more importantly, added five extra components to the chip, therefore, increasing the minimum size required. Finally, the most common way to increase the bandwidth because of its simplicity is simply adding a quarter-wave transformer to port-1 of the combiner. This results in matching the impedances between the output port and the symmetrical quarter-wave transformers.

3.1 Multistage Wilkinson Junction

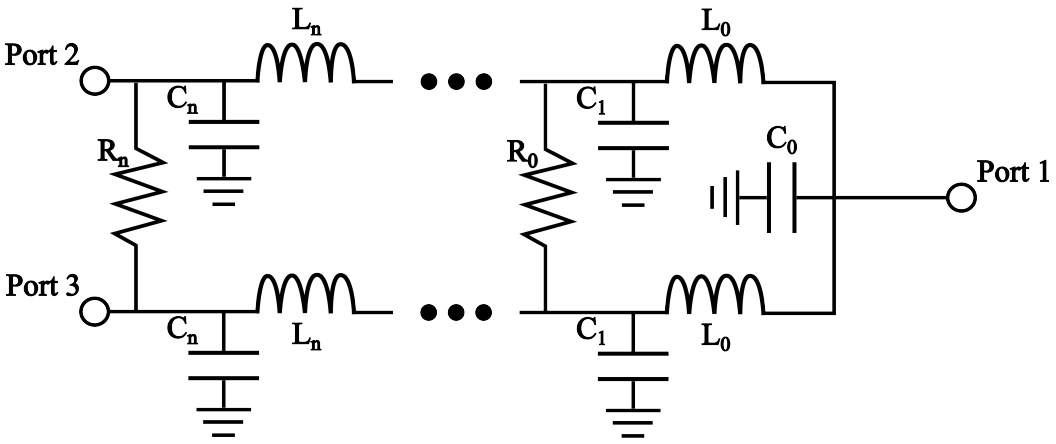

Figure 7: Multistage Wilkinson junction circuit diagram.

Pictured in Fig. 7 is the most common method for expanding the bandwidth at each stage of the Wilkinson junction consisting of one quarter-wave transformer for each branch of the Wilkinson junction and one more resistor. There is no direct solution for detuning this. However, there are several common methods for finding an optimal solution. There is a common solution for a single-frequency dual-band Wilkinson power splitter where $R_0 = 40\ \Omega$ and $R_2 = 125\ \Omega$ we then set $Z_1 = 100\ \Omega$ and $Z_2 = Z_1/\sqrt{2}$. This is shown for a 15 MHz circuit in Fig. 8. Comparing the relative bandwidths from the Fig. 6, we can immediately see a larger bandwidth, but also of note is that the multistage simulation, along with the actual circuits on the higher frequency side, agrees with the normalized analytical solution and the lower frequency sections disagree. This is because the analytical solution has a mirroring effect that does not occur in either the simulations or experimentally. This is because of the process of normalizing the frequency rather than a limitation in solving for the bandwidth using ABCD matrices.

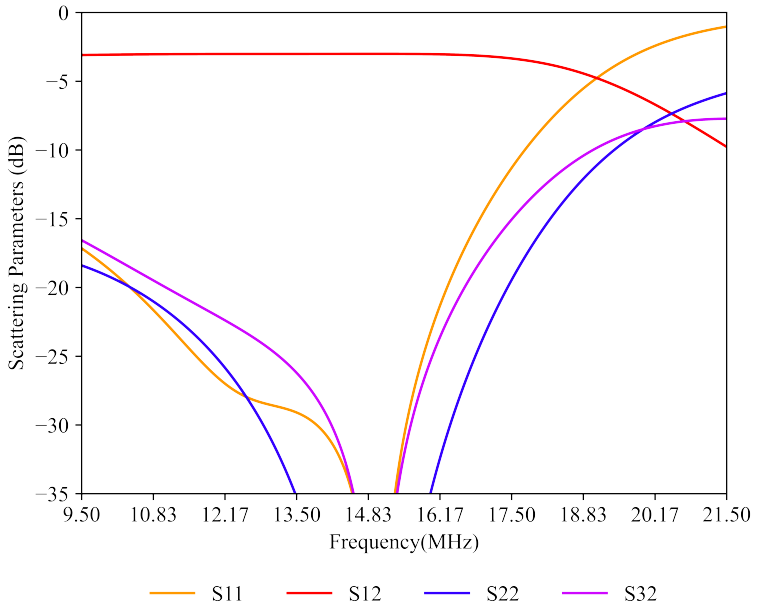

Figure 8: Multistage simulation of relevant scattering parameters. A clear natural frequency is observed at 15MHz where five of the relevant scattering parameters become zero and S_{12}, S_{13}, S_{21}, S_{31} are reduced to half the power, -3 dB. The upper bound of the natural frequency is located at 16.9 MHz, shown by the dashed gray line.

This solution is for the ideal multistage Wilkinson junction with a single natural frequency. It is a prevalent method to detune the natural frequencies, trading isolation for the bandwidth of the device.

3.2 Leading Quarter-wave Wilkinson Junction

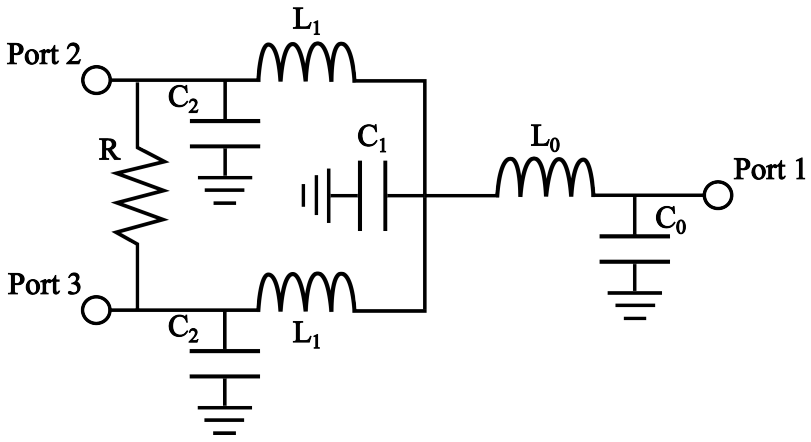

Figure 9: Leading quarter-wave Wilkinson junction circuit diagram.

For the simplest method to increase the Wilkinson combiners bandwidth, we can add a characteristic impedance quarter-wave transformer at the output port. This will reduce the number of reflections at the ports. In Fig. 10, we can see that there is a larger bandwidth than the single-stage Wilkinson junction with a minimal amount of work and a minimal amount of added space on the chip.

This design is also used by Elsbury in *Broadband Lumped-Element Integrated N-Way Power Dividers for Voltage Standards* for a programmable Josephson voltage standard [4]. This is a similar application we would desire for the final use of the Wilkinson junction, giving us confidence that the device would be manufactured. It is also the same magnitude as the frequency of interest for the proposed Haloscope design, having been designed for 20 GHz rather than the 15.7 GHz where the axion is suspected to be located [2].

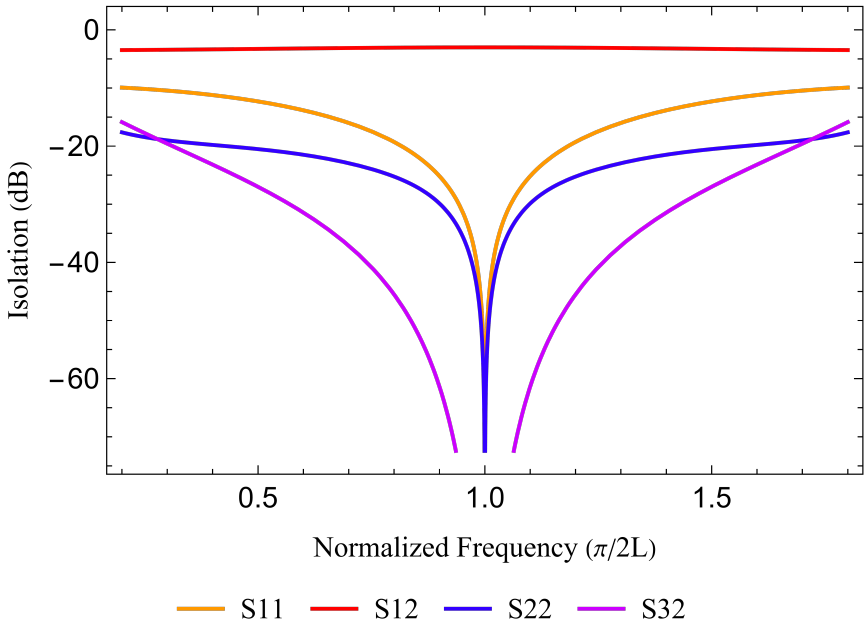

Figure 10: Leading quarter-wave Wilkinson junction with a matched quarter-wave transformer. This shows a moderate improvement on the single-stage Wilkinson junctions scattering parameters as shown in Fig. 6 with minimal work.

The goal is now to detune the Wilkinson junction's natural frequency. This is done by numerical optimization. Unfortunately, when using the simplex method or other standard methods, a bounding problem arises where natural frequencies are found, creating deep spikes rather than a desired flat curve. In the perfect case for the Wilkinson junction, we would see a horizontal line at the half power line, -3 dB, and all other scattering parameters at $-\infty$ dB for as long as possible. Because we are interested in testing the optimization method, we have chosen a challenging but achievable -15 dB isolation as our goal.

The numerical optimization follows a simple procedure where we iteratively separate the relative frequencies of the quarter-wave transformers until a peak is formed at the central frequency. We can change the impedances of the quarter-wave transformers and resistors.

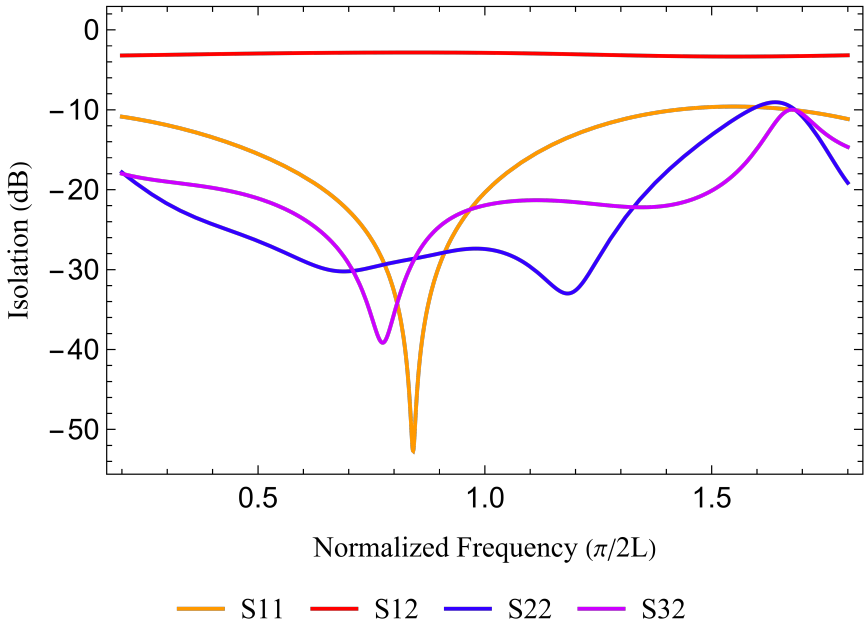

Figure 11: Detuned Wilkinson junction analytical solution created using the ABCD scattering matrix analytical solution and numerical optimization. From the above, we can see that there are two natural frequencies, neither of which will go to the infinite isolation seen in Fig. 6 or Fig. 8.

Repeating this numerical optimization can find a testable set of parameters. These values come to the quarter-wave impedances being changed to 98.15% and 99.00% of their initial values from the design with one natural frequency. We then find the relative frequencies of the two sets of quarter-wave transformers and a potential solution at 116.53% and 123.20% of their initial values. Finally, we see a satisfying answer when the resistor is 92% of the original value. This provides the plot Fig. 11.

4 Testing and Concept Validation

With the values found for the detuned Wilkinson junction in the previous section, we can finish our design by using Microwave Office from AWR to simulate the circuit at a frequency of interest. We now must determine how to design for a frequency of interest. Due to the added difficulties with superconducting circuits and higher-frequency devices, we decided to scale down from Buschmann's identified frequency of 15.7 GHz to 15 MHz. This scaling down allows for the construction of room-temperature components and commercial solutions for inductors, capacitors, and resistors. To test this concept, we will compare a detuned leading quarter-wave transformer Wilkinson junction and a traditionally calculated leading quarter-wave transformer Wilkinson junction.

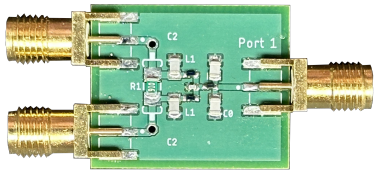

Figure 12: Detuned Wilkinson junction surface mount PCB. This is a 15 MHz-centered experimental validation of detuning the different parts of the Wilkinson junction to increase usable bandwidth.

The final circuit of the detuned Wilkinson junction is shown in Fig. 12 where all inductors, capacitors, and resistors are readily commercially available. The low frequency also allowed us to use Fr4 for the PCB substrate.

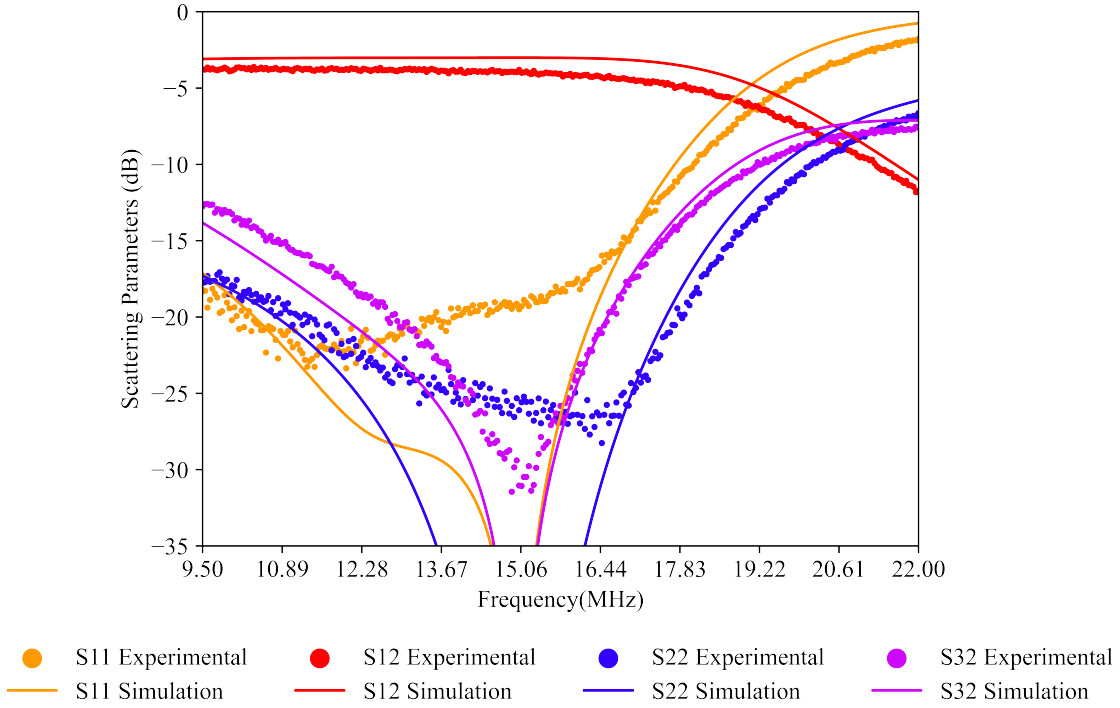

Figure 13: Leading Wilkinson junction simulation plotted against experimental data scatter plotted. We see a strong correlation between the simulated and experimental data. This shows that the experimental data has an approximate bandwidth of 6 MHz.

In Fig. 13, We can see that the simulated and experimental data both go to a single natural frequency with the required -15 dB isolation going from 10.8 MHz to 16.8 MHz for the physical device. This was a confirmatory test that our simulations worked appropriately and had a solid background analytically.

Compared to Fig. 14, we can see that the data is flatter than the traditionally calculated Wilkinson junction at the chosen isolation.

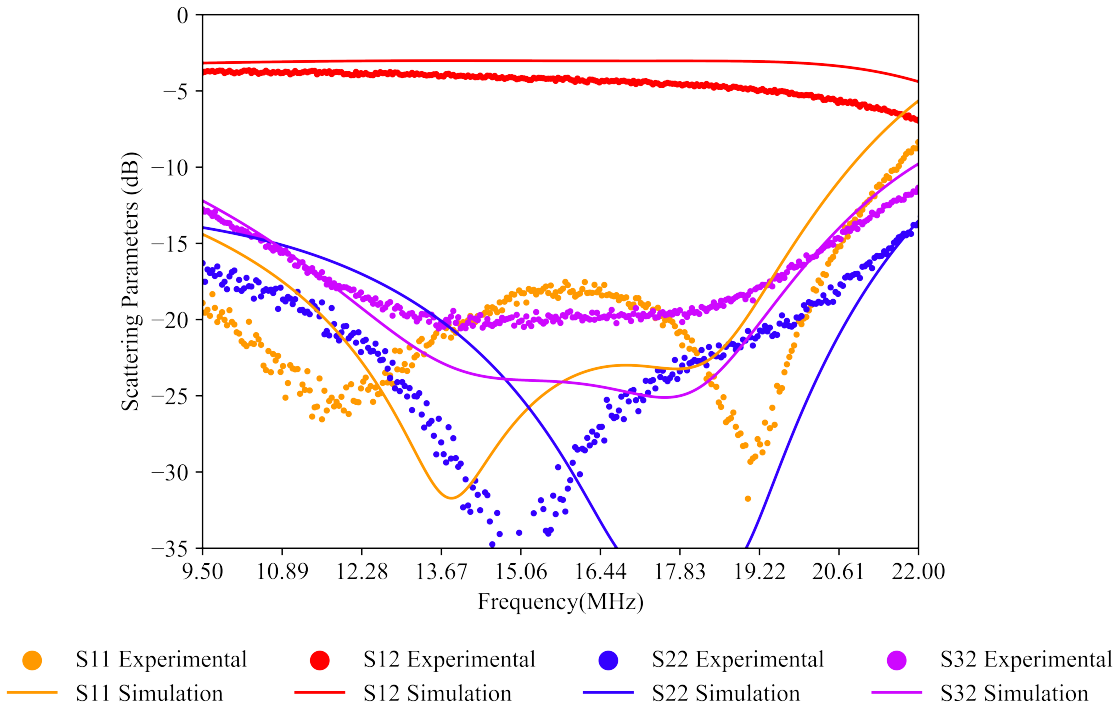

Figure 14: Detuned Wilkinson junction simulation plotted against the analytical solution. The experimental data show a stronger correlation with the natural frequencies than was predicted using AWR. A large bandwidth of approximately 10 MHz was measured for the device.

With the detuned Wilkinson junction, we can see a large bandwidth starting at 10.9 MHz and going to 20.9 MHz. We also see an expected weaker amount of isolation than the simulated data, for which further analysis will be required to adjust the design properly. We see a defined natural frequency for S_{22} in both the experimental data and simulated solution. We also see that the observed and simulated data offset each other at the current moment. It is unclear what is the most significant cause of the mismatched data. We believe that most of the differences are due to surface mount component tolerances requiring further testing and manufacturing to confirm.

5 Conclusion

In this thesis, we have motivated the potential need for Wilkinson junctions in designing a plasma haloscope and reviewed the primary literature on Wilkinson junctions. We then tested the potential of detuning the Wilkinson junction, which showed promising results in increasing the

potential bandwidth while maintaining the same circuit and manufacturing complexity. In this first iteration, we have demonstrated a substantial improvement of approximately 66% on the original design. The detuned leading quarter-wave transformer offers a promising start. However, the multistage device simulated is still expected to have a higher usable bandwidth. It is left to future consideration to determine if the added complexity on the chip and on-chip size or the bandwidth is of more importance for the correct function of a plasma haloscope.

The future work on Wilkinson junctions includes making a higher frequency model centered at Buschmann's identified frequency of interest, 15.7 GHz. If this test is passed, a large binary tree of Wilkinson junctions can be constructed and characterized. With this circuit, we can compare the losses of a traditionally designed Wilkinson junction tree and the detuned model.

References

[1] L. F. Abbott and P. Sikivie. A cosmological bound on the invisible axion. *Physics Letters B*, 120(1):133–136, 1983.

[2] Malte Buschmann, Joshua W. Foster, and Benjamin R. Safdi. Early-universe simulations of the cosmological axion. *Phys. Rev. Lett.*, 124:161103, Apr 2020.

[3] N. Du, N. Force, R. Khatiwada, E. Lentz, R. Ottens, L. J Rosenberg, G. Rybka, G. Carosi, N. Woollett, D. Bowring, A. S. Chou, A. Sonnenschein, W. Wester, C. Boutan, N. S. Oblath, R. Bradley, E. J. Daw, A. V. Dixit, J. Clarke, S. R. O'Kelley, N. Crisosto, J. R. Gleason, S. Jois, P. Sikivie, I. Stern, N. S. Sullivan, D. B Tanner, and G. C. Hilton. Search for invisible axion dark matter with the axion dark matter experiment. *Phys. Rev. Lett.*, 120:151301, Apr 2018.

[4] Michael M. Elsbury, Paul D. Dresselhaus, Norman F. Bergren, Charles J. Burroughs, Samuel P. Benz, and Zoya Popovic. Broadband Lumped-Element Integrated N-Way Power Dividers for Voltage Standards. *IEEE Transactions on Microwave Theory and Techniques*, 57(8):2055–2063, August 2009. Conference Name: IEEE Transactions on Microwave Theory and Techniques.

[5] Jui-Chih Kao, Zuo-Min Tsai, Kun-You Lin, and Huei Wang. A modified wilkinson power divider with isolation bandwidth improvement. *IEEE Transactions on Microwave Theory and Techniques*, 60(9):2768–2780, 2012.

[6] Masahiro Kawasaki, Ken'ichi Saikawa, and Toyokazu Sekiguchi. Axion dark matter from topological defects. *Phys. Rev. D*, 91:065014, Mar 2015.

[7] Vincent B. Klaer and Guy D. Moore. The dark-matter axion mass. *Journal of Cosmology and Astroparticle Physics*, 2017(11):049, nov 2017.

[8] Tove Klaesson. *Computational simulations of the Axion Longitudinal Plasma HAloscope*. PhD thesis, Stockholm University, 2023.

[9] Matthew Lawson, Alexander J. Millar, Matteo Pancaldi, Edoardo Vitagliano, and Frank Wilczek. Tunable axion plasma haloscopes. *Physical Review Letters*, 123(14):141802, October 2019. arXiv: 1904.11872.

[10] Ely Levine and Haim Matzner. Calculating scattering parameters of wilkinson power dividers via abcd matrices [speaker's corner]. *IEEE Microwave Magazine*, 22(11):82–88, 2021.

[11] Alexander J. Millar, Steven M. Anlage, Rustam Balafendiev, Pavel Belov, Karl van Bibber, Jan Conrad, Marcel Demarteau, Alexander Droster, Katherine Dunne, Andrea Gallo Rosso, Jon E. Gudmundsson, Heather Jackson, Gagandeep Kaur, Tove Klaesson, Nolan Kowitt, Matthew Lawson, Alexander Leder, Akira Miyazaki, Sid Morampudi, Hiranya V. Peiris, Henrik S. Røising, Gaganpreet Singh, Dajie Sun, Jacob H. Thomas, Frank Wilczek, Stafford Withington,

Mackenzie Wooten, Jens Dilling, Michael Febbraro, Stefan Knirck, Claire Marvinney, and Endorsers. Searching for dark matter with plasma haloscopes. *Physical Review D*, 107(5):055013, March 2023.

[12] R. D. Peccei and Helen R. Quinn. CP conservation in the presence of pseudoparticles. *Phys. Rev. Lett.*, 38:1440–1443, Jun 1977.

[13] J. B. Pendry, A. J. Holden, D. J. Robbins, and W. J. Stewart. Low frequency plasmons in thin-wire structures. *Journal of Physics: Condensed Matter*, 10(22):4785–4809, June 1998. Publisher: IOP Publishing.

[14] David M Pozar. *Microwave engineering; 3rd ed.* Wiley, Hoboken, NJ, 2005.

[15] John Preskill, Mark B. Wise, and Frank Wilczek. Cosmology of the invisible axion. *Physics Letters B*, 120(1):127–132, 1983.

[16] P. Sikivie. Experimental tests of the "invisible" axion. *Phys. Rev. Lett.*, 51:1415–1417, Oct 1983.

[17] Steven Weinberg. A new light boson? *Phys. Rev. Lett.*, 40:223–226, Jan 1978.

[18] F. Wilczek. Problem of strong p and t invariance in the presence of instantons. *Phys. Rev. Lett.*, 40:279–282, Jan 1978.

[19] E.J. Wilkinson. An N-Way Hybrid Power Divider. *IRE Transactions on Microwave Theory and Techniques*, 8(1):116–118, January 1960. Conference Name: IRE Transactions on Microwave Theory and Techniques.